Parameter inference from X-ray spectral modeling of thermal tidal disruption events

Richard Saxton

Andrew Mummery,Thomas Wevers, Andy Read, Kate Alexander, Dongyue Li, Giovanni Miniutti, Margherita Giustini, Jari Kajava

Image credit: ESO/ M. Kornmesser

TDE disks are bigger than they seem:

Simple blackbody modeling provides good quality of fit, but strongly biased parameter constraints

One cannot infer physical parameters (e.g. black hole mass, spin, bolometric disk luminosity) from spectral modeling

Mummery (2021) used a Laplace expansion of general relativistic thin disk equations to describe soft (kT < 0.2 keV) thermal disk emission in TDEs

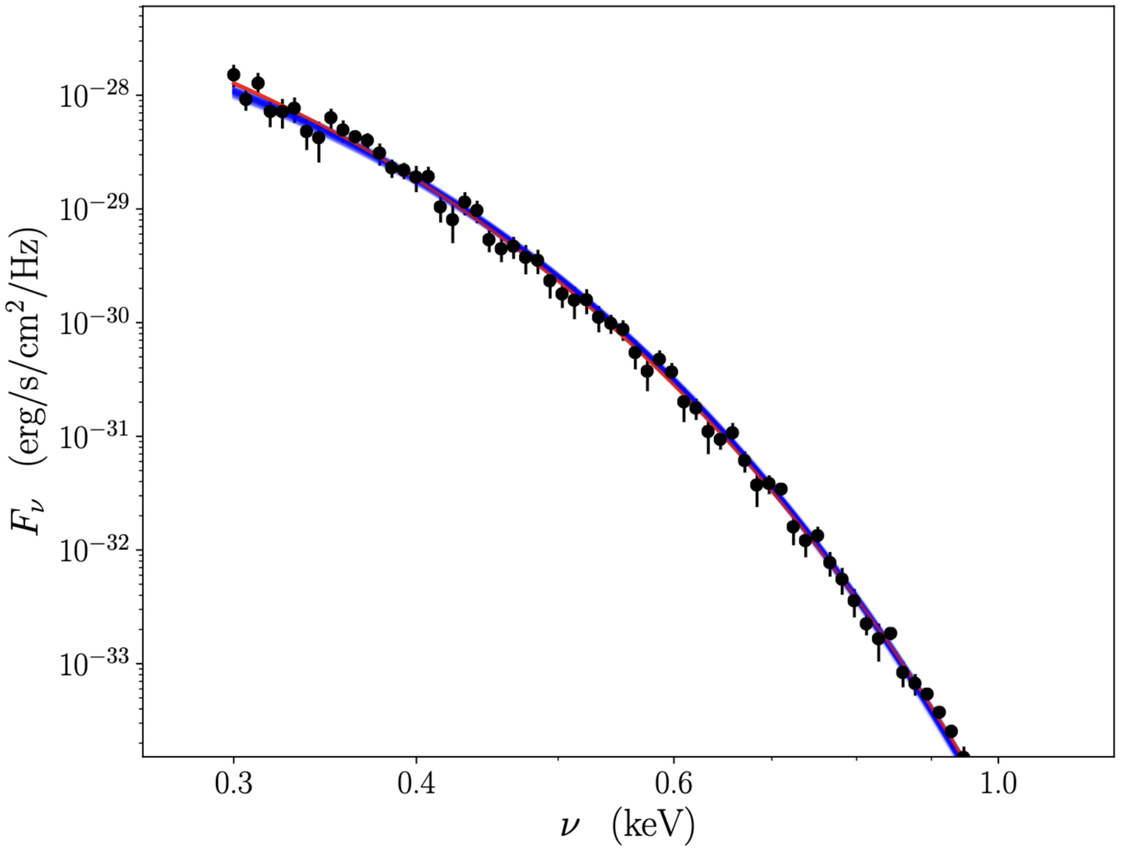

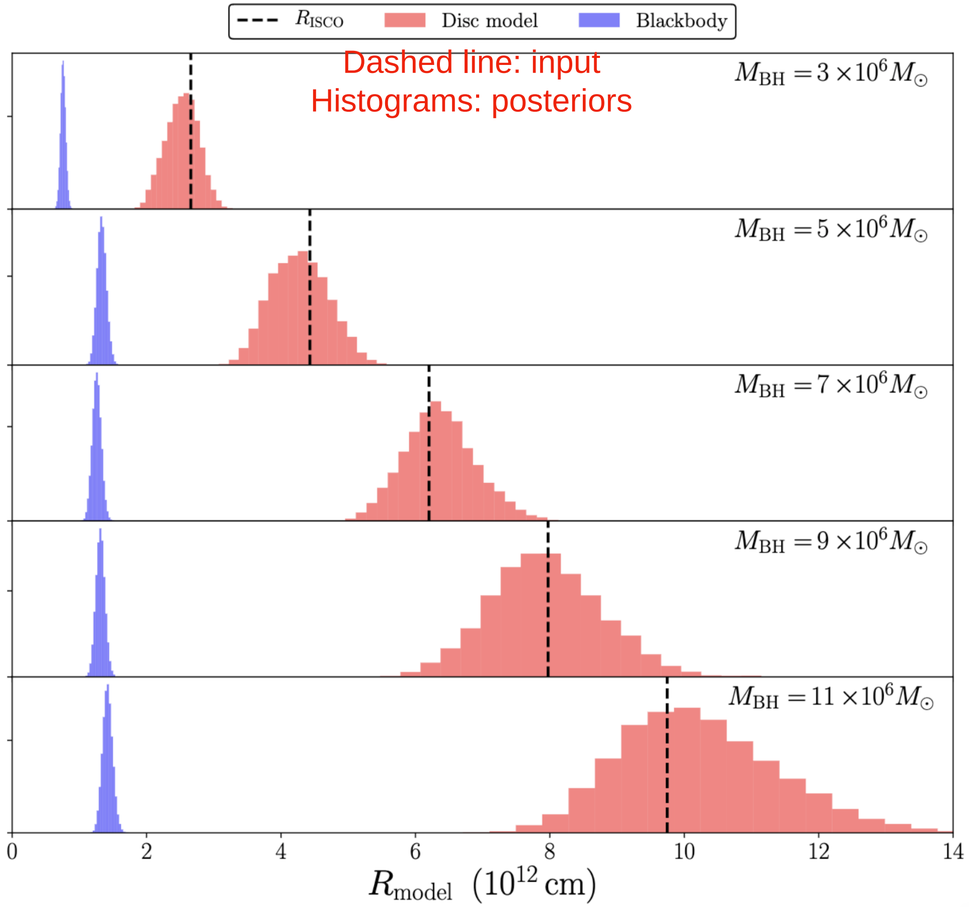

Simulation of a thermal spectrum and the recovered parameters using spectral fitting

Analytical fit to the Wien tail

In the Wien-tail limit,
use Laplace expansion of
relativistic thin disk model
about the hottest disk region

Model described by only 3 parameters:
R_p, T_p, gamma

T_p: hottest temperature in the disk

R_p: physical location of T_p (ISCO)

gamma (nuisance parameter) :
disk inclination and
inner boundary condition

$$F_\nu(R_p, \widetilde{T}_p) = \frac{4\pi\xi_1 h\nu^3}{c^2 f_{\rm col}^4}\left(\frac{R_p}{D}\right)^2\left(\frac{k\widetilde{T}_p}{h\nu}\right)^\gamma \exp\left(-\frac{h\nu}{k\widetilde{T}_p}\right) \times\left[1+\xi_2\left(\frac{k\widetilde{T}_p}{h\nu}\right)+\xi_3\left(\frac{k\widetilde{T}_p}{h\nu}\right)^2+\ldots\right], \quad (6)$$

- Model only valid for low temperatures kT~<200 eV
- Model behaviour when PL present not calibrated
- Colour correction from Done+2012 model
- Valid for Eddington ratios 0.01 < f_edd < 1
- Xspec implementation publicly available

Mummery et al. 2023, MNRAS, 519, 5828

Image credit: ESO/ M. Kornmesser

With this model, we can infer parameters for a sample of TDEs!
But first, collate and curate the X-ray data

Publicly available X-ray data (exluding ROSAT)

Too high temperature, or strong power-law present

Too low photon statistics (<100 counts)

Source	RA	Dec.	Redshift	Distance (Mpc)	Galactic n_H (10^{20} cm^{-2})	σ (km/s)	Reference
ASASSN–14li	12 48 15.23	17 46 26.4	0.0206	90	1.9	78 ± 2	[1], [2]
ASASSN–15oi	20 39 09.03	–30 45 20.8	0.051	216	4.8	61±7	[3], [4], [5]
~~OGLE16aaa~~	~~01 07 20.88~~	~~–64 16 20.7~~	~~0.1655~~	~~800~~	~~2.7~~	—	~~[6], [7]~~
AT2019dsg	20 57 02.974	+14 12 15.86	0.0512	224	6.5	94 ± 1	[8], [24]
AT2018zr	07 56 54.54	+34 15 43.61	0.071	322	4.4	—	[9]
~~AT2018fyk~~	~~22 50 16.09~~	~~–44 51 53.50~~	~~0.059~~	~~264~~	~~1.15~~	~~158±1~~	~~[10], [11]~~
~~3XMM J1500~~	~~15 00 52.07~~	~~+01 54 53.8~~	~~0.145~~	~~692~~	~~4.1~~	~~59±3~~	~~[12]~~
~~XMMSL1 J0740~~	~~07 40 08.09~~	~~–85 39 31.3~~	~~0.0173~~	~~73~~	~~5.3~~	~~112± 3~~	~~[13], [11]~~
3XMM J1521	15 21 30.72	+07 49 16.5	0.179	866	2.7	58±2	[14]
GSN069	01 19 08.663	–34 11 30.52	0.018	69	2.3	64 ± 4	[15]
~~SDSSJ1201~~	~~12 01 36.03~~	~~+30 03 05.5~~	~~0.146~~	~~700~~	~~1.3~~	~~122±4~~	~~[16]~~
~~XMMSL2 J1446~~	~~14 46 05.22~~	~~+68 57 31.1~~	~~0.029~~	~~127~~	~~1.7~~	~~167 ±15~~	~~[17], [11]~~
2XMM J1847	18 47 25.12	–63 17 25.3	0.035	156	6.3	91±4	[18]
~~AT2018lyz~~	~~10 06 50.871~~	~~+01 41 34.08~~	~~0.0457~~	~~204~~	~~2.7~~	~~57 ± 1~~	~~[19]~~
~~RBS1032~~	~~11 47 26.69~~	~~+49 42 57.7~~	~~0.026~~	~~114~~	~~1.4~~	~~49 ± 7~~	~~[20]~~
AT2019azh	08 13 16.95	+22 38 54.03	0.022	96	4.2	77 ± 2	[21]
2MASX J0249	02 49 17.31	–04 12 52.1	0.019	83	3.2	43 ± 4	[20]
~~AT2019qiz~~	~~04 46 37.88~~	~~–10 13 34.90~~	~~0.0151~~	~~66~~	~~6.6~~	~~71 ± 2~~	~~[22]~~
AT2020ksf	21 35 27.26	–18 16 35.54	0.0923	426	3.6	—	[23]

Reduced data (XMM-Newton, Swift, NICER) available on Zenodo!

DOI: 10.5281/zenodo.7533374

ASASSN-14li
ASASSN-15oi
OGLE16aaa
AT2019dsg
AT2018zr
3XMM J1521
GSN 069
2XMM J1847
AT2019azh
2MASX J0249
AT2020ksf

Source	Instrument	Photon counts	MJD (days)	Spectral range (keV)	n_H (10^{20} cm^{-2})	R_p (10^{12} cm)	T_p (10^5 K)	γ	Fit statistic (stat/d.o.f.)
ASASSN–14li	XMM/RGS	9200	56997	0.35 – 1.2	$6.1^{+2.2}_{-1.5}$	$6.1^{+3.7}_{-0.5}$	$3.7^{+0.6}_{-0.1}$	0.5	353/266
ASASSN–14li	XMM/RGS	36150	56999	0.35 – 1.2	$4.6^{+0.8}_{-0.7}$	$4.8^{+0.8}_{-0.2}$	$3.8^{+0.2}_{-0.1}$	0.5	1267/873
ASASSN–14li	XMM/RGS	9600	57024	0.35 – 1.2	$6.5^{+1.4}_{-1.2}$	$6.4^{+1.7}_{-0.4}$	$3.6^{+0.2}_{-0.04}$	0.5	378/269
ASASSN–14li	XMM/RGS	2086	57213	0.35 – 1.2	$4.0^{+0.5}_{-0.5}$	$4.8^{+4.5}_{-0.7}$	$3.2^{+0.6}_{-0.1}$	0.5	79/72
ASASSN–14li	XMM/RGS	5700	57367	0.35 – 1.2	$4.0^{+0.5}_{-0.5}$	$5.2^{+4.1}_{-0.7}$	$3.0^{+0.4}_{-0.1}$	0.5	222/232
ASASSN–14li	XMM/PN	22400	57399	0.2 – 1.0	$3.7^{+0.9}_{-0.4}$	$5.1^{+1.5}_{-0.3}$	$2.9^{+0.4}_{-0.1}$	0.5	214/157
ASASSN–14li	XMM/PN	18400	57544	0.2 – 1.0	$3.9^{+0.6}_{-0.5}$	$6.0^{+1.6}_{-0.4}$	$2.6^{+0.2}_{-0.1}$	0.5	171/157
ASASSN–14li	XMM/PN	9800	57727	0.2 – 1.0	$3.9^{+0.8}_{-0.6}$	$6.2^{+3.2}_{-0.5}$	$2.5^{+0.3}_{-0.2}$	0.5	133/157
ASASSN–14li	XMM/PN	8200	57912	0.2 – 1.0	$3.7^{+0.9}_{-0.8}$	$8.0^{+6.1}_{-0.7}$	$2.2^{+0.4}_{-0.1}$	0.5	129/157
ASASSN–14li	XMM/PN	7600	58093	0.2 – 1.0	$1.5^{+0.8}_{-0.6}$	$2.6^{+2.4}_{-0.2}$	$2.5^{+0.4}_{-0.2}$	0.5	175/157
ASASSN–15oi	XMM/PN	600	57324	0.2 – 1.0	$4.8^{\dagger}$	$0.58^{+0.22}_{-0.16}$	$5.0^{+0.5}_{-0.7}$	1.5	139/157
ASASSN–15oi	XMM/PN	4050	57482	0.2 – 1.0	$4.8^{\dagger}$	$2.8^{+0.8}_{-0.3}$	$3.3^{+0.3}_{-0.1}$	0.5	179/157
OGLE16aaa	XMM/PN	260	57548	0.2 – 1.0	$3.3^{+3.4}_{-3.3}$	$1.7^{+1.4}_{-0.8}$	$4.1^{+1.9}_{-1.2}$	0.5	112/157
OGLE6aaa	XMM/PN	4500	57722	0.2 – 1.0	$1.3^{+0.6}_{-0.9}$	$1.5^{+0.5}_{-0.6}$	$6.1^{+0.4}_{-1.1}$	0.5	173/157
AT2019dsg	NICER	13000	58624	0.3 – 1.0	$8.6^{+1.4}_{-0.8}$	$1.8^{+1.3}_{-0.3}$	$4.9^{+0.8}_{-0.1}$	0.5	10.5/13
AT2019dsg	NICER	3800	58625	0.3 – 1.0	$10.0^{+1.7}_{-3.1}$	$2.8^{+1.4}_{-1.4}$	$5.6^{+0.5}_{-0.9}$	1.5	14/12
AT2019dsg	NICER	1300	58630	0.3 – 1.0	$8.1^{+2.4}_{-0.7}$	$1.8^{+2.8}_{-0.5}$	$4.8^{+1.2}_{-0.5}$	0.5	8/12
AT2019dsg	NICER	750	58633	0.3 – 1.0	$9.1^{+2.9}_{-1.1}$	$2.3^{+4.7}_{-0.9}$	$4.5^{+1.3}_{-0.5}$	1.4	13/12
AT2019dsg	NICER	660	58634	0.3 – 1.0	$6.3^{+2.7}_{-0.8}$	$1.1^{+1.9}_{-0.5}$	$5.0^{+1.7}_{-0.6}$	0.6	10/11
AT2018zr	XMM/PN	300	58220	0.2 – 1.0	$14.3^{+2.7}_{-3.3}$	$0.071^{+0.040}_{-0.036}$	$9.5^{+0.3}_{-1.1}$	1.5	198/157
AT2018zr	XMM/PN	185	58242	0.2 – 1.0	$17.1^{+8.9}_{-5.1}$	$0.095^{+0.045}_{-0.040}$	$8.7^{+0.5}_{-2.2}$	1.5	165/157
3XMM J1521	XMM/PN	3050	51778	0.2 – 1.2	$2.1^{+1.3}_{-0.8}$	$0.32^{+0.03}_{-0.03}$	$8.2^{+1.7}_{-0.5}$	0.5	232/198
GSN 069	XMM/PN	55000	56996	0.2 – 1.0	$3.3^{+0.3}_{-0.3}$	$0.67^{+0.06}_{-0.02}$	$3.8^{+0.2}_{-0.05}$	0.5	256/158
2XMM J1847	XMM/PN	2000	53985	0.2 – 1.2	$6.3^{\dagger}$	$0.20^{+0.03}_{-0.03}$	$7.5^{+0.4}_{-0.4}$	1.5	176/175
2XMM J1847	XMM/PN	18000	54206	0.2 – 1.2	$9.6^{+0.4}_{-0.8}$	$0.55^{+0.05}_{-0.07}$	$8.2^{+0.2}_{-0.4}$	1.5	254/198
AT2019azh	Swift	240	58553 - 58634	0.3 – 10	$5.4^{+8.0}_{-5.3}$	$0.6^{+3.8}_{-0.5}$	$4.3^{+1.8}_{-1.5}$	1.5	90/82
AT2019azh	Swift	2500	58767 - 58977	0.3 – 10	$4.2^{\dagger}$	$1.4^{+1.1}_{-0.1}$	$3.8^{+1.0}_{-0.05}$	0.5	55/65
2MASX J0249	XMM/PN	1780	53930	0.2 – 1.2	$31.8^{+10.2}_{-3.8}$	$0.23^{+0.52}_{-0.09}$	$6.8^{+1.6}_{-0.6}$	0.5	260/219
AT2020ksf	NICER	14450	59187 - 59189	0.3 – 1.5	$3.3^{+1.4}_{-0.6}$	$0.8^{+0.3}_{-0.05}$	$7.5^{+1.0}_{-0.1}$	0.5	22/22
AT2020ksf	NICER	11230	59191 - 59195	0.3 – 1.4	$6.2^{+1.0}_{-0.9}$	$1.7^{+0.5}_{-0.2}$	$5.7^{+0.4}_{-0.2}$	0.5	27/19
AT2020ksf	Swift	440	59179 - 59205	0.3 – 1.5	$5.2^{+6.2}_{-3.5}$	$1.1^{+2.1}_{-0.5}$	$6.3^{+2.1}_{-0.7}$	0.5	45/65

Results 1: $T_p \propto R_p^{-1/4}$

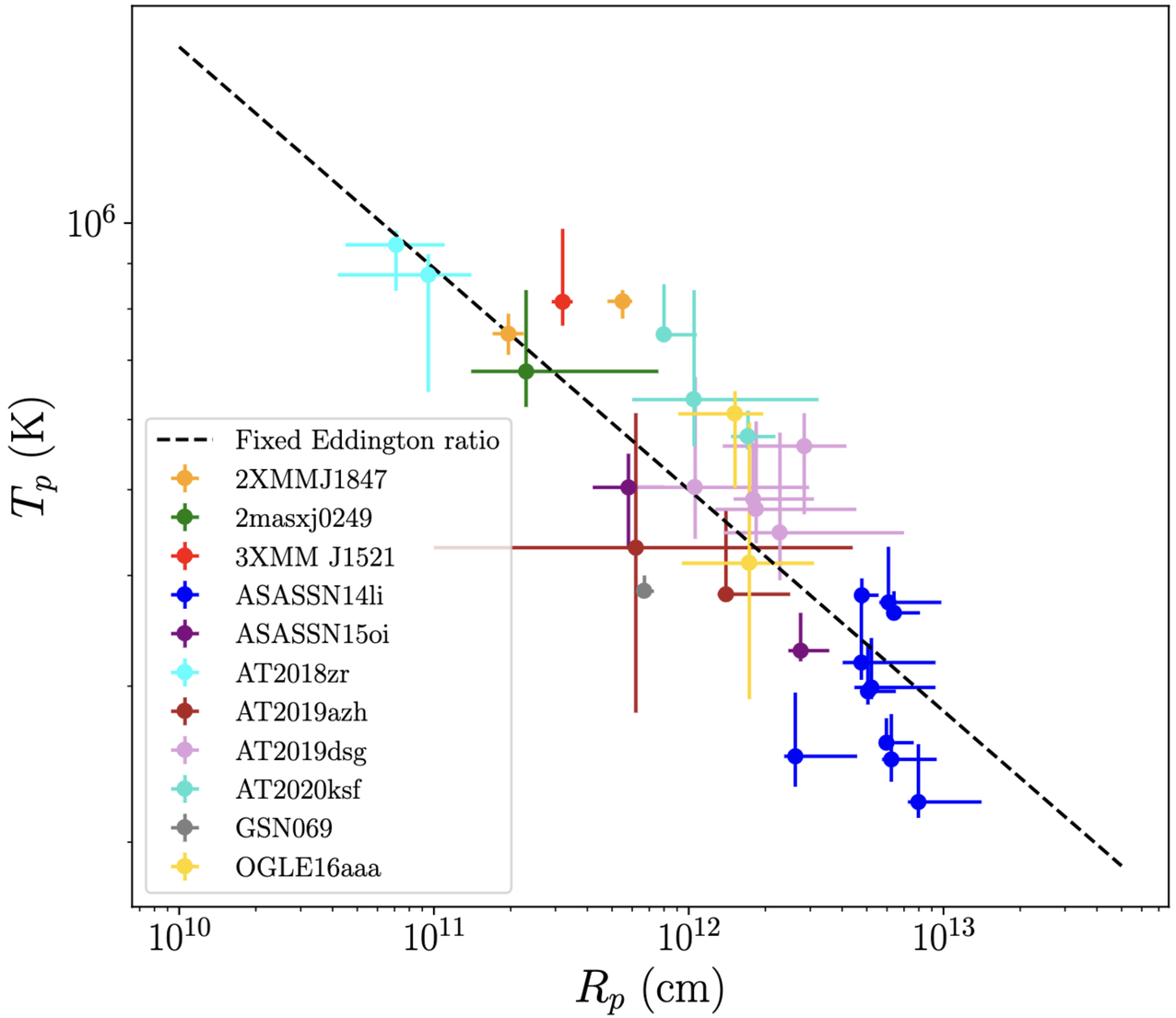

Expected if radius scales linearly with black hole mass, and Eddington ratio is more or less constant

Results 2: bolometric disk luminosity

Because the disk model is known analytically, integration over frequency yields bolometric disk luminosity

L_bol is proportional to $R_p^2 T_p^4$

Positive correlation between
M-sigma black hole mass and L_bol

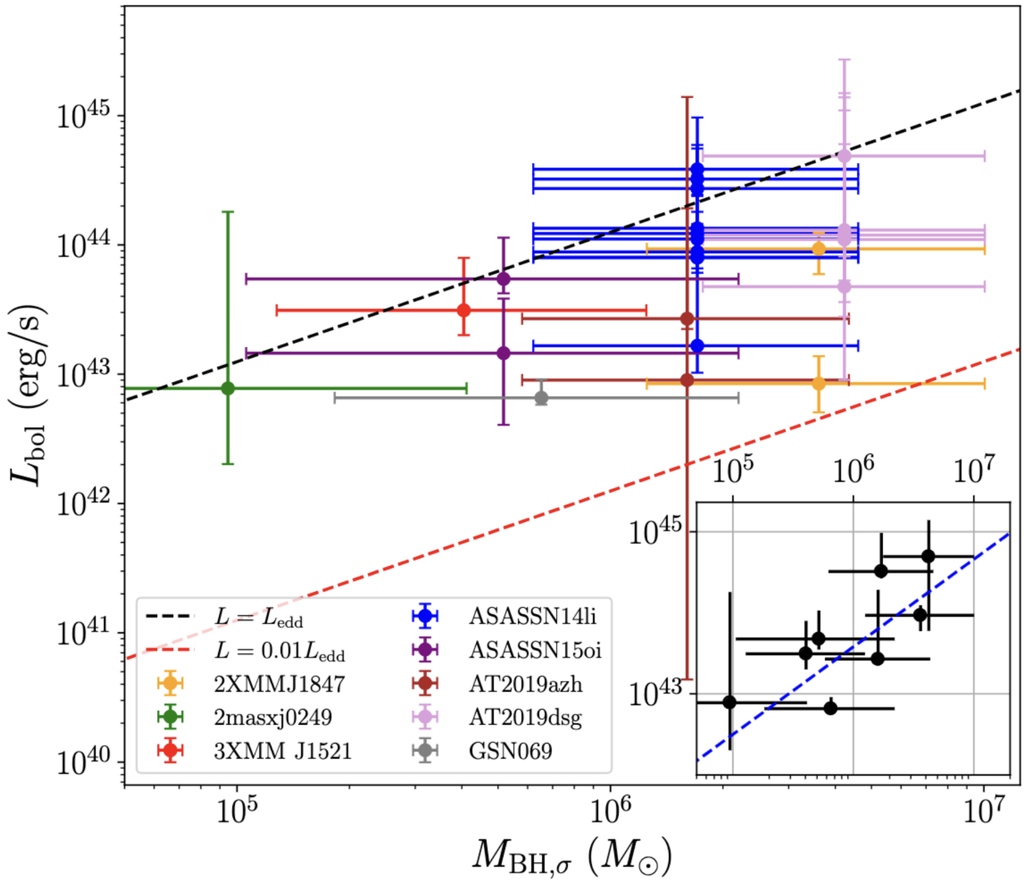

This correlation is NOT driven by obscuration

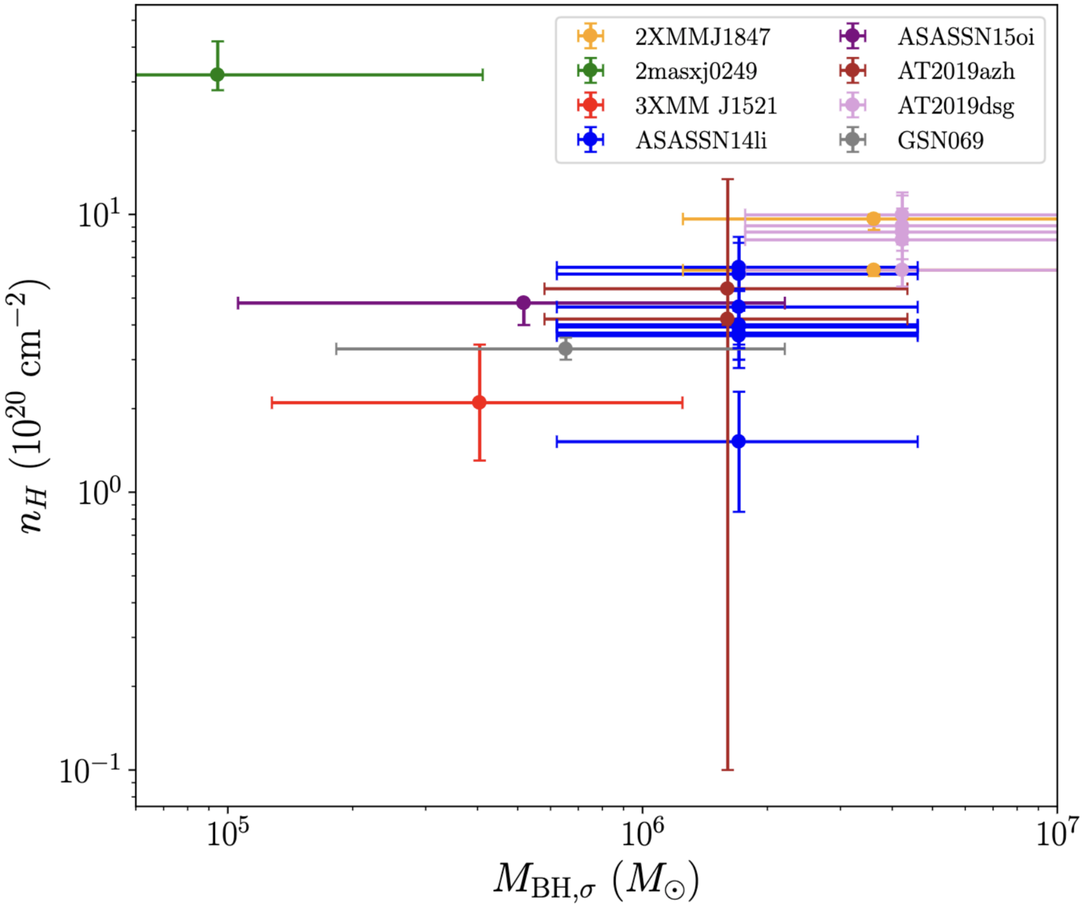

Results 3: temperature dependent bolometric correction

Can reach values up to 100!

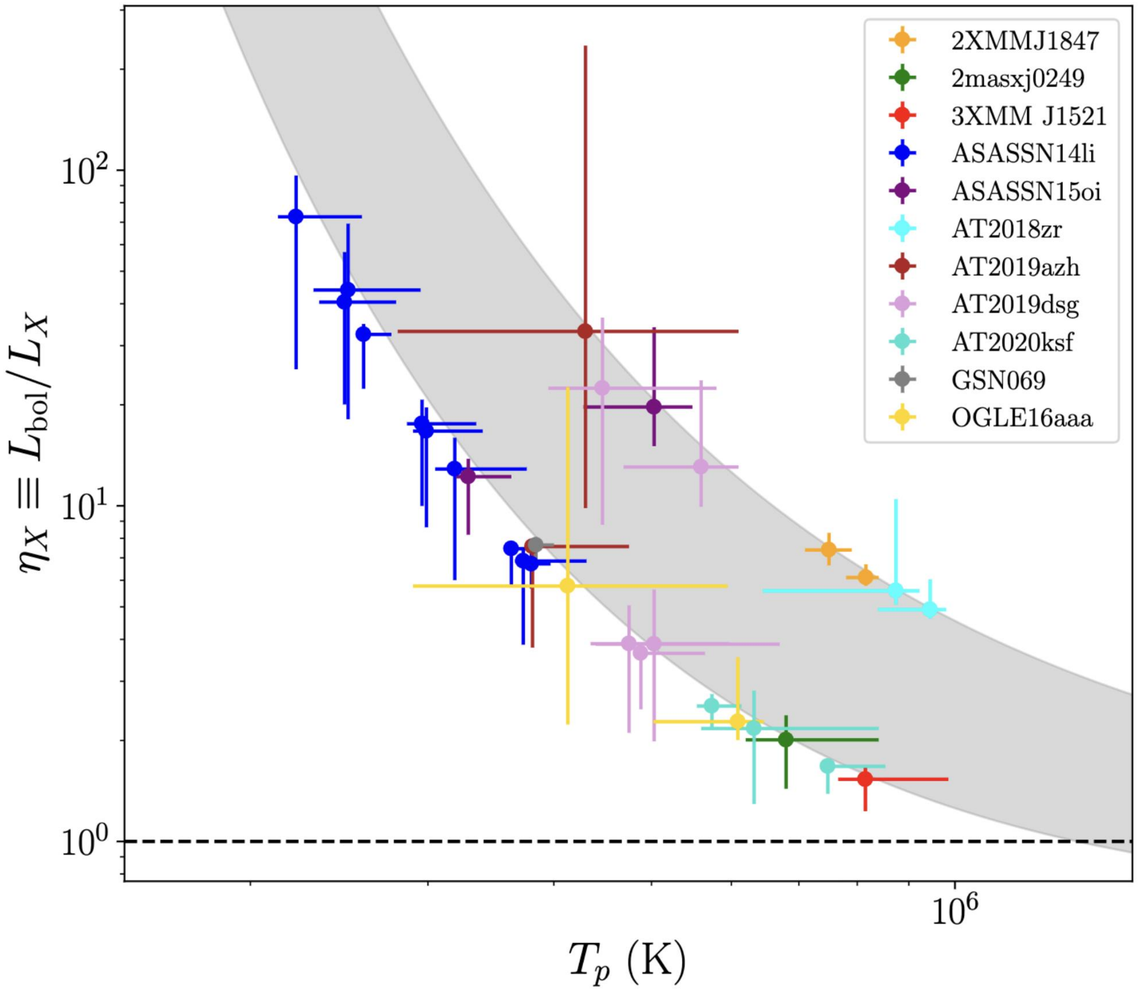

Example: ASASSN-14li X-ray lightcurve

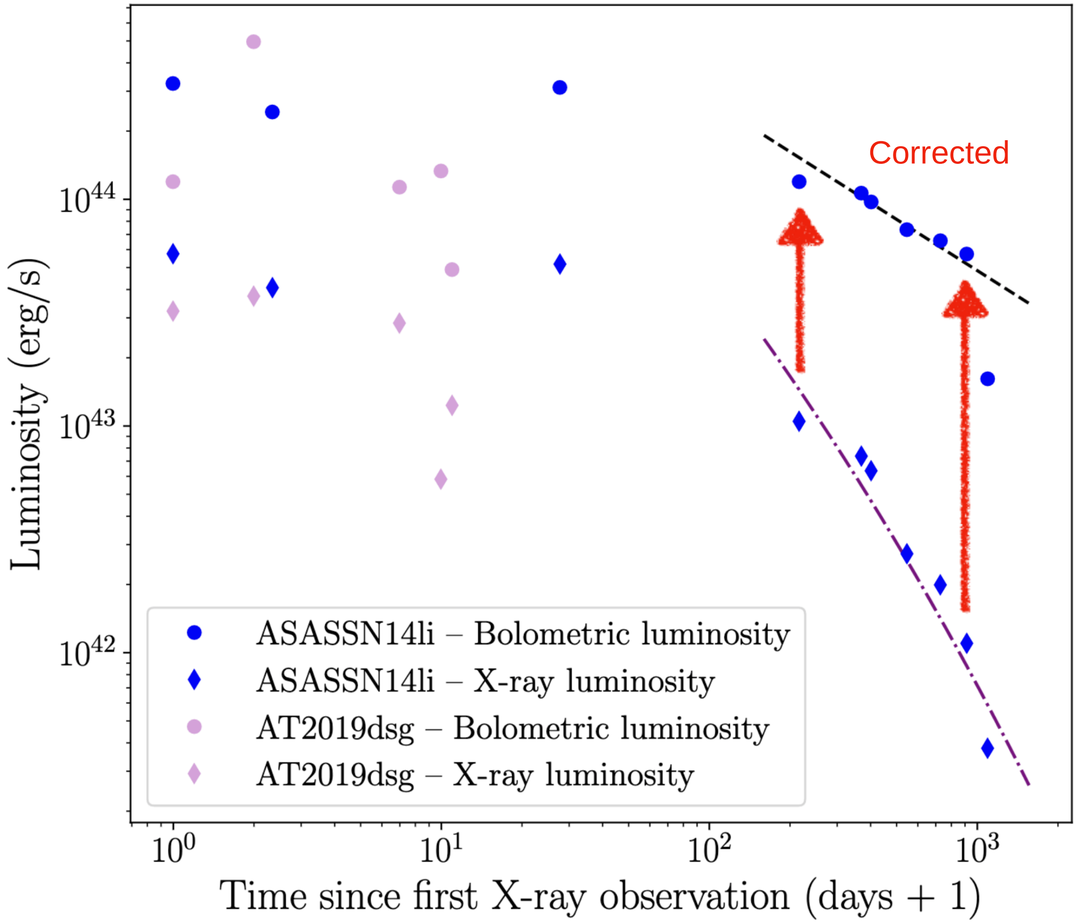

Explains the surprisingly low inferred accreted mass (“missing energy problem”)!

Real accreted mass

M_tot=0.11 M_solar

Results 4: inferring black hole mass

R_p tracks the ISCO radius inferred from M-sigma relation

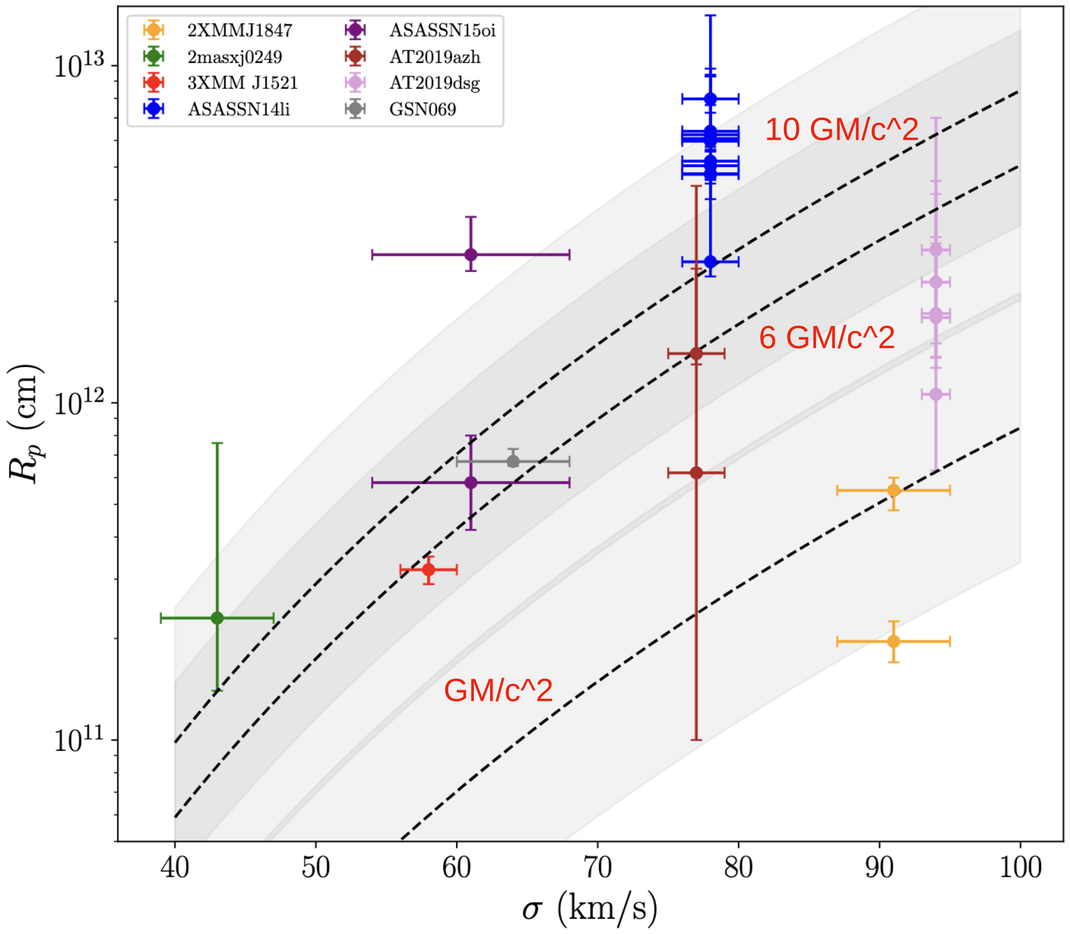

BUT: degenerate with disk inclination and BH spin

Simulate a wide range of inclinations and spins to assess effect:
Generate thin disk, ray-trace temperature profile, fit X-ray spectrum

Ratio of R_ISCO (input) to R_p (measured)

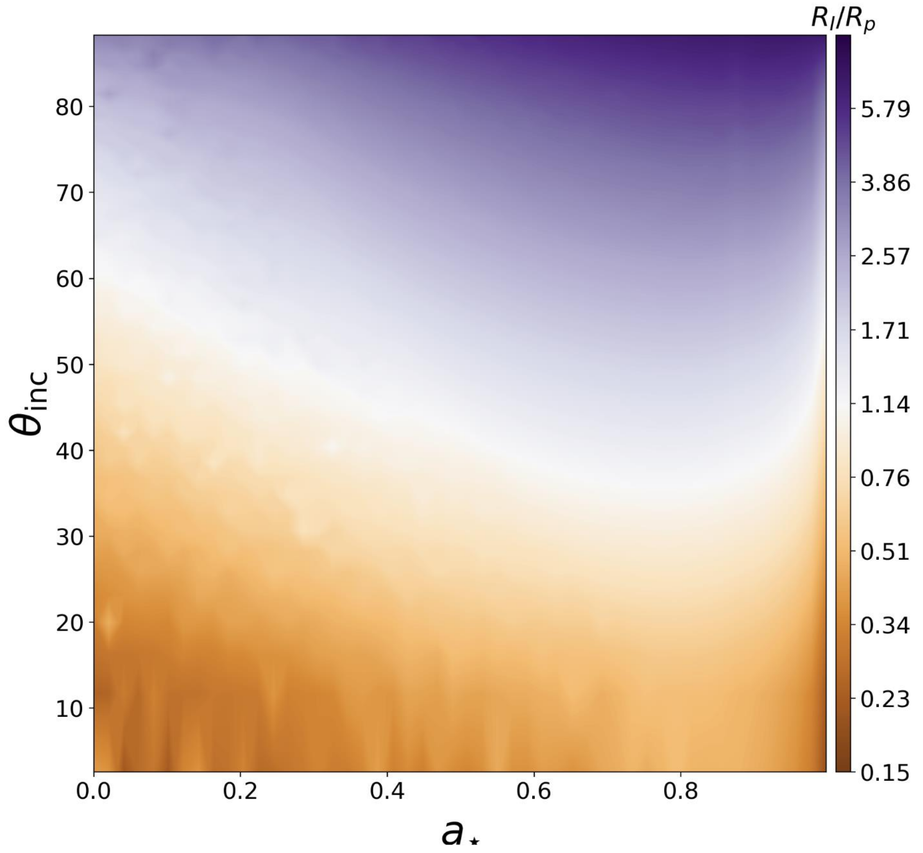

$$\left(\frac{M_{\mathrm{BH},R_p}}{10^6 M_\odot}\right) = X\left(\frac{R_p}{10^{12}\,\mathrm{cm}}\right). \qquad \overline{X} \simeq 4.9^{+7.1}_{-3.0},$$

Results 5: origin of the UV/optical luminosity

If UV/optical luminosity is powered by reprocessing X-rays, then always L_UV/opt < L_disk_bol

Source	$L_{\mathrm{BB,max}}$ (erg/s)	$L_{\mathrm{disc,max}}$ (erg/s)	$L_{\mathrm{BB,max}} / L_{\mathrm{disc,max}}$	Δt (days)	Reference
ASASSN-14li	1.0×10^{44}	3.1×10^{44}	0.32	41	Holoien et al. 2016a
ASASSN-15oi	1.3×10^{44}	4.8×10^{43}	2.7	234	Holoien et al. 2016b
""	""	1.45×10^{43}	9.0	76	""
OGLE16aaa	2.1×10^{44}	2.1×10^{44}	1.0	315	van Velzen et al. 2021
""	""	5.6×10^{43}	3.75	141	""
AT2018zr	5.6×10^{43}	3.7×10^{42}	15.1	40	van Velzen et al. 2021
AT2019azh	2.8×10^{44}	2.7×10^{43}	10.4	200	van Velzen et al. 2021
""	""	9.0×10^{42}	31.1	30	""
AT2019dsg	2.9×10^{44}	4.9×10^{44}	0.59	18	van Velzen et al. 2021

This is not always the case, so for these sources L_UV/opt cannot be solely reprocessing-powered!
There must be an additional energy injection mechanism that contributes to the UV/optical luminosity (e.g. stream shocks)

Or we are missing significant absorption in the spectral fits ?

TDE: XMMSL2 J1404-25

Discovery image – 15/02/2018

Atel #11394

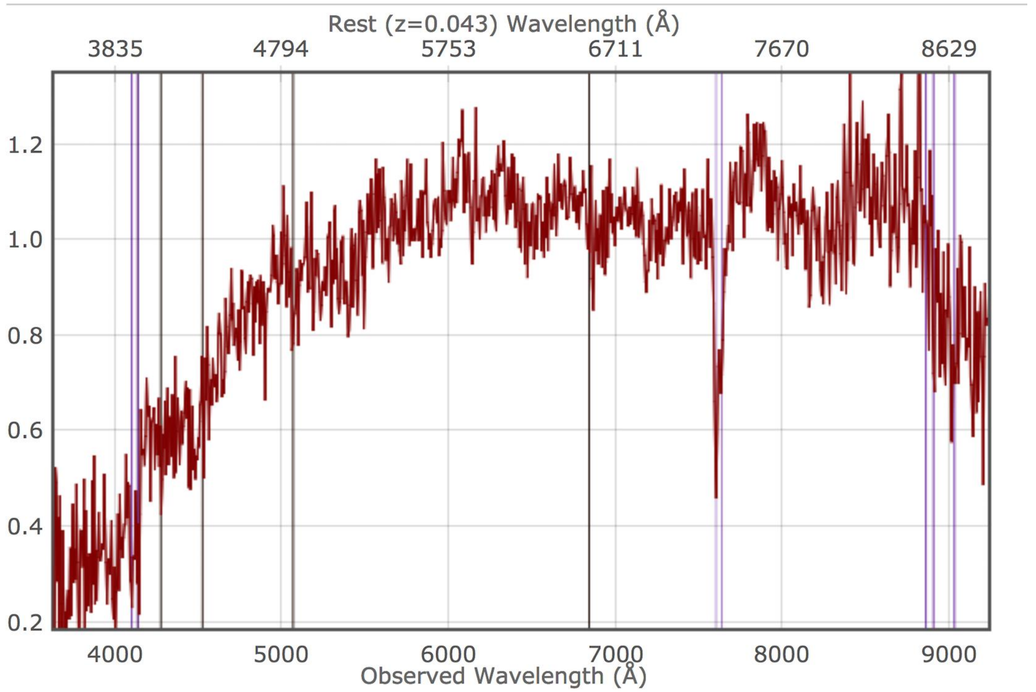

ePESSTO NTT, EFOSC2 spectrum (8 Mar 2018)
Atel #11395

>20 brighter than ROSAT in 1990

2MASX 1404671-1511433

z=0.043

Saxton et al. in prep

2MASX 1404-25: creation of corona

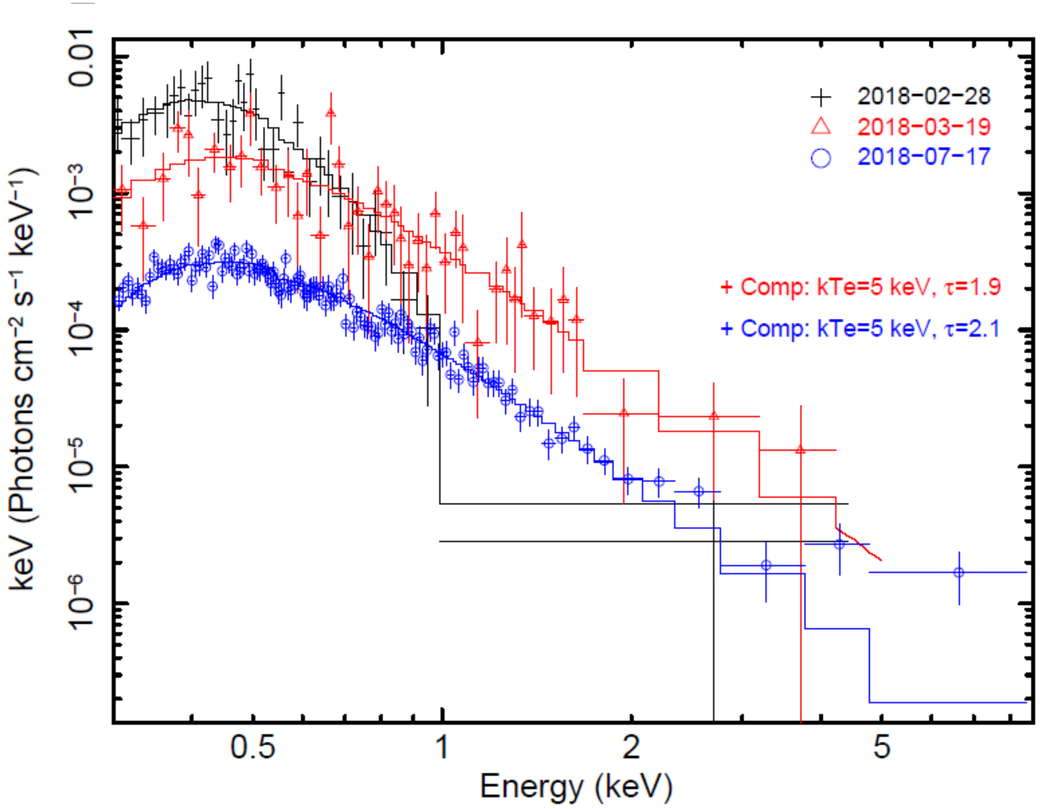

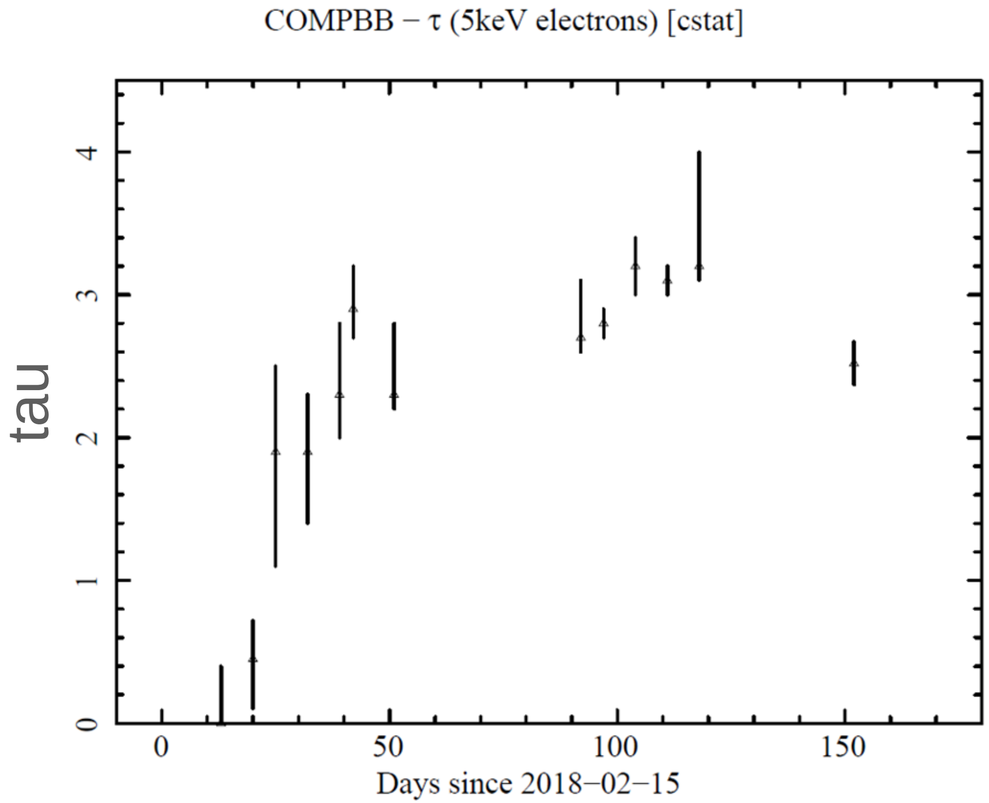

Comptonisation:

tau=1.9, kTe=5 keV, developed within 7 days.

Corona creation occurs at m_dot=0.05 – 0.5 m_edd

Fast but 50x too slow to explain QPEs !

2MASS 1404-25 : very steep decay

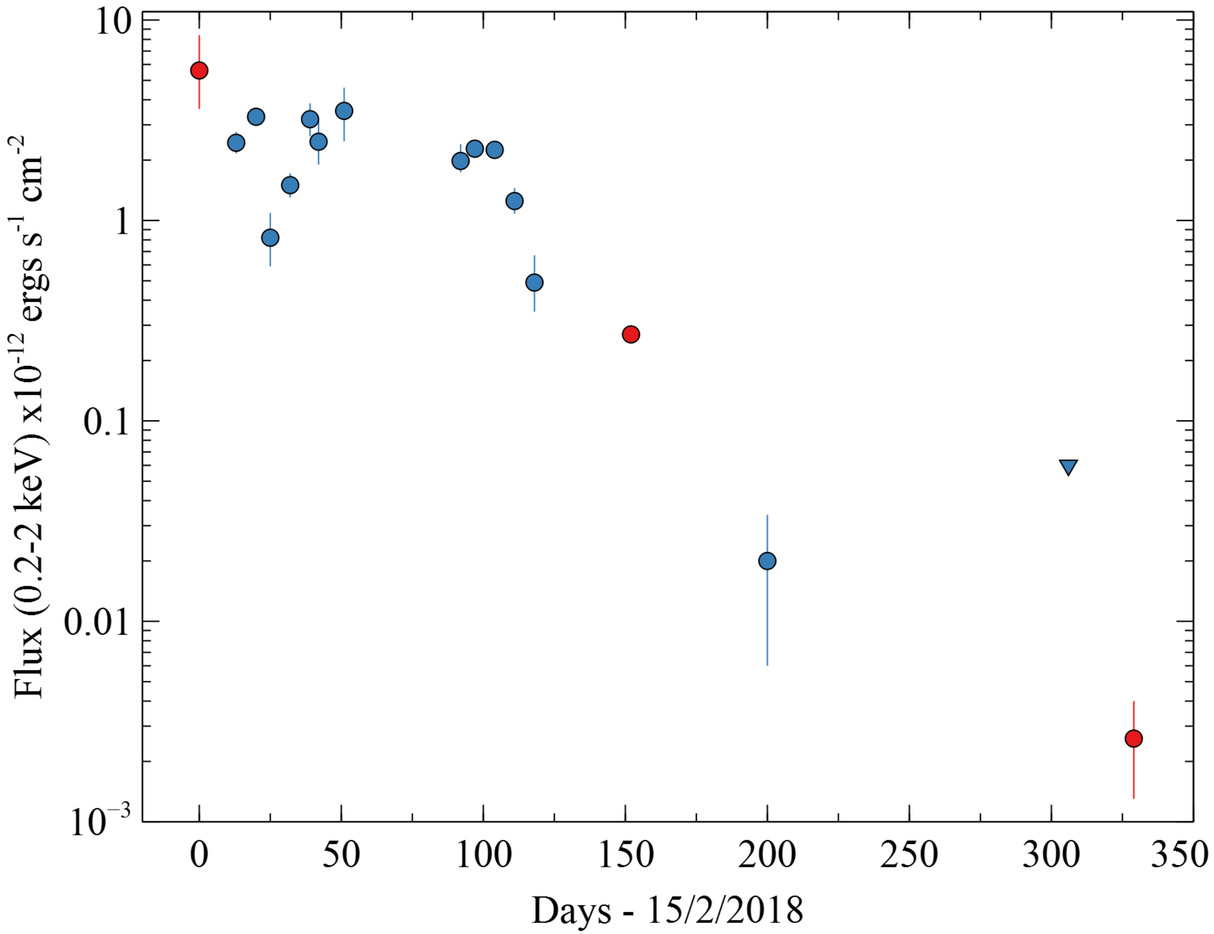

Soft X-ray flux decay of ~2000 in 330 days

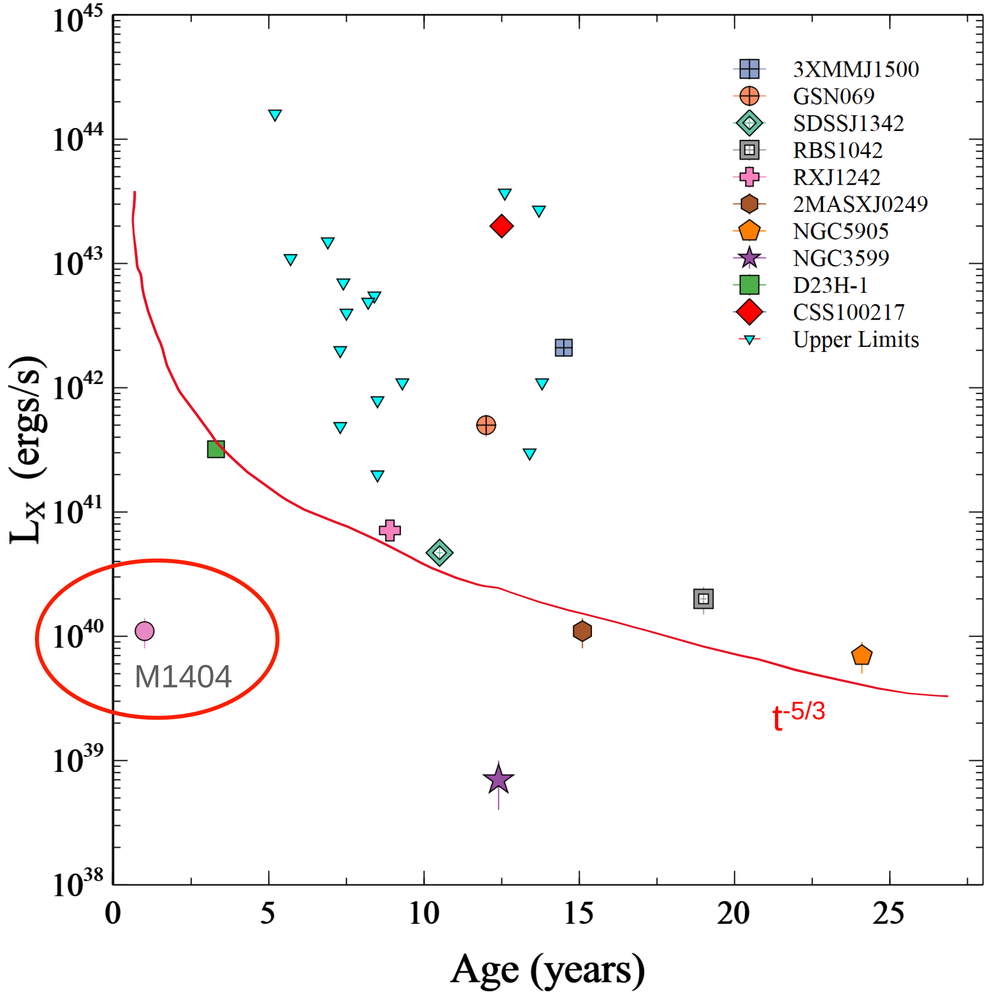

Late-time X-ray luminosities

Bolometric correction for disc+corona

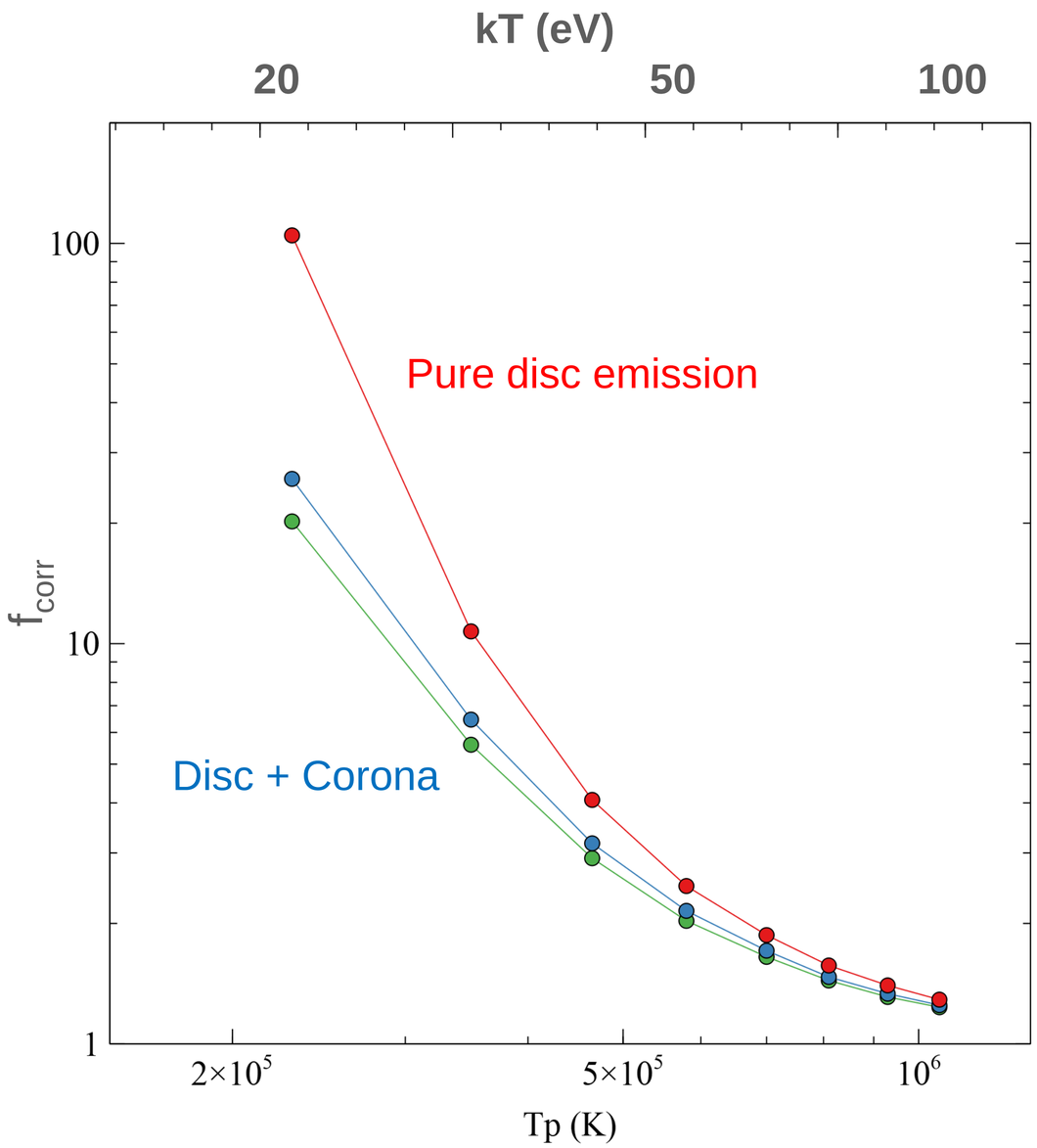

X-ray and Bolometric lightcurves for 2MASS 1404-25

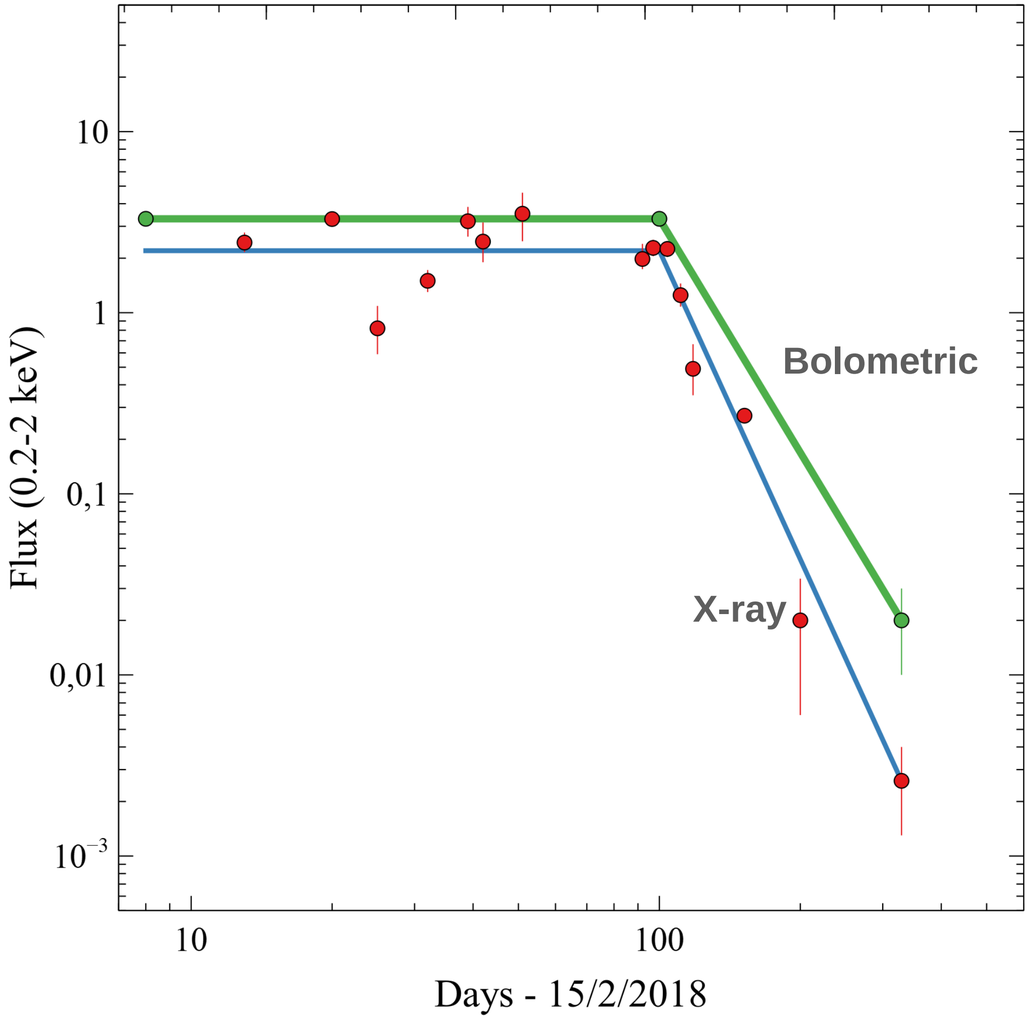

MCG+07-34-146

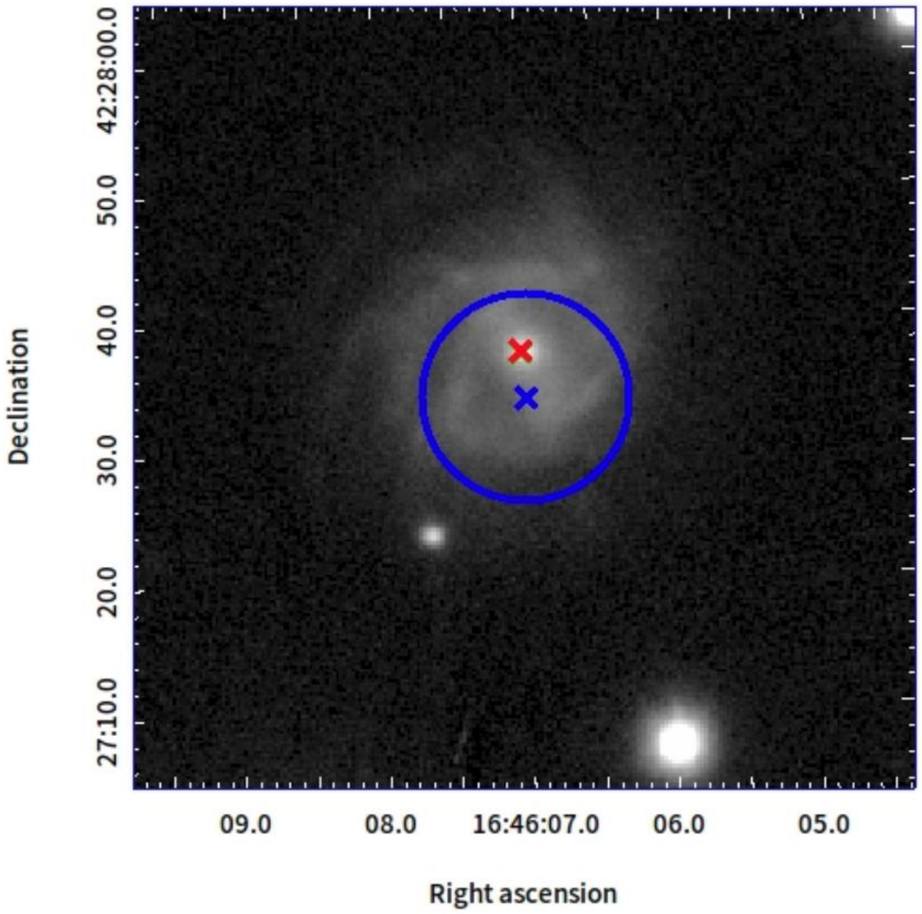

optical image, z=0.049
red: optical
blue: XMMSL position and error circle

optical spectra, starforming galaxy

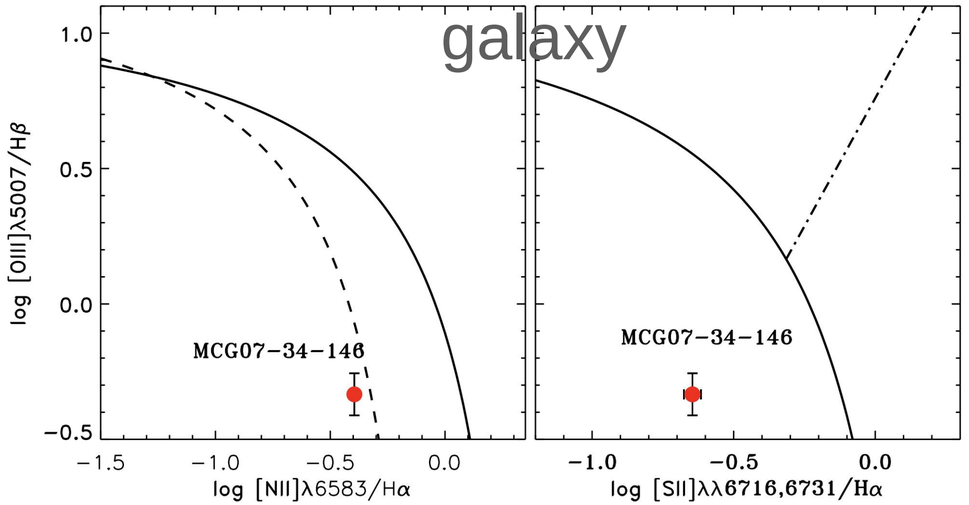

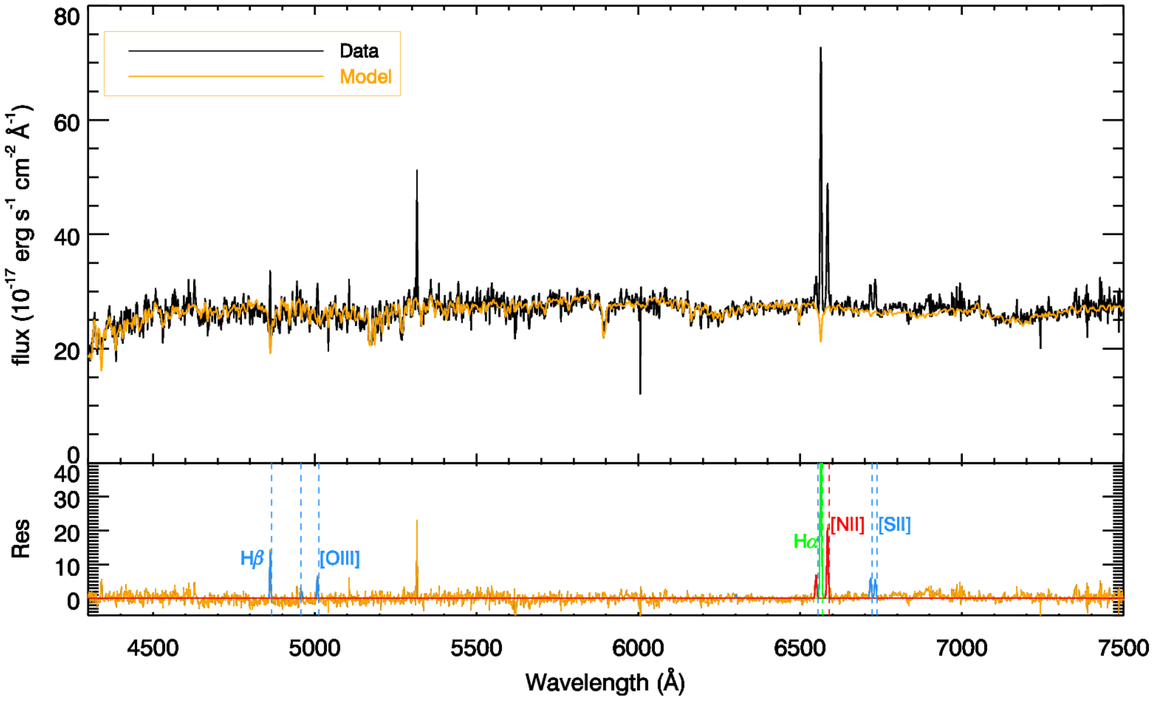

MCG+07-34-146

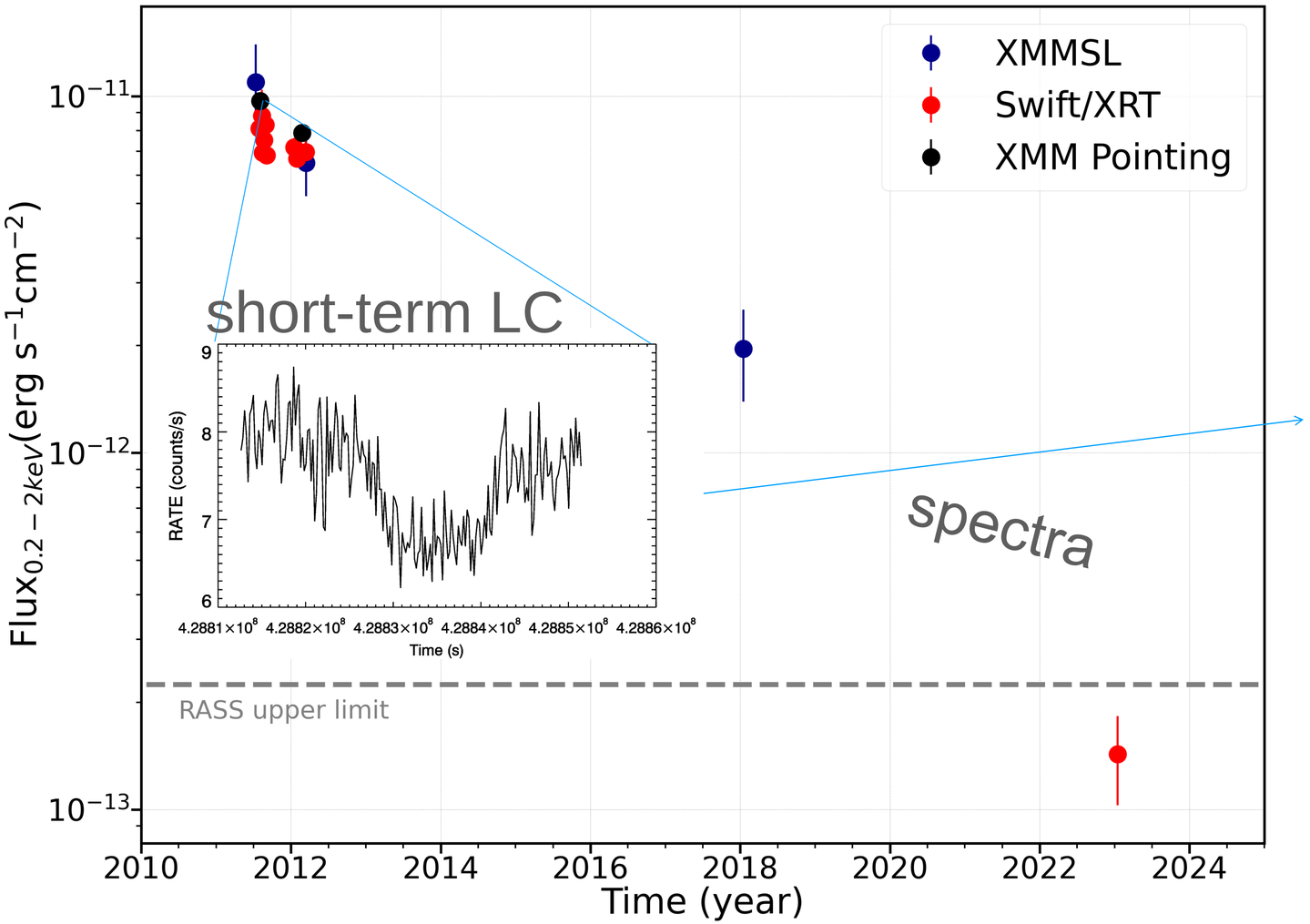

X-ray spectra fitted with: tbabs*(zbb+zpo)

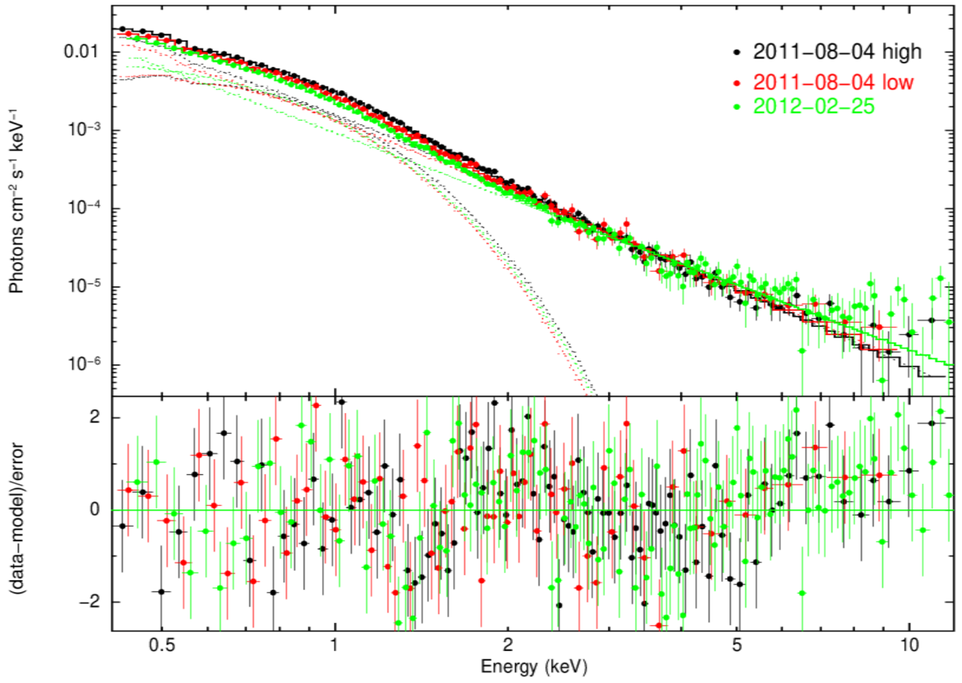

Li et al. in prep

Conclusions

1. Purely thermal TDEs, if realistically modelled, can give a competitive M_BH measurement

$$\left(\frac{M_{\mathrm{BH},R_p}}{10^6 M_\odot}\right) = X\left(\frac{R_p}{10^{12}\,\mathrm{cm}}\right).$$

$$\overline{X} \simeq 4.9^{+7.1}_{-3.0},$$

2. The lack of X-ray absorption features and limited bolometric disc luminosity in TDEs with a bright UV/optical peak challenges the reprocessing model

3. X-ray TDEs with fast creation of spectral components – can help to constrain disc mechanisms and help to fill in the TDE parameter space little by little